Journal of Catalysis 268 (2009) 282–289

Contents lists available at ScienceDirect

Journal of Catalysis

journal homepage: www.elsevier.com/locate/jcat

Suppression of CO by-production in steam reforming of methanol by addition of zinc oxide to silica-supported copper catalyst

Yasuyuki Matsumura [a,*], Hideomi Ishibe [b]

[a] National Institute of Advanced Industrial Science and Technology (AIST) Kansai Center, Midorigaoka, Ikeda, Osaka 563-8577, Japan
[b] Nippon Seisen Co. Ltd., Hirakata Plant, Ikenomiya, Hirakata, Osaka 573-8522, Japan

ARTICLE INFO

Article history:
Received 30 June 2009
Revised 25 September 2009
Accepted 26 September 2009
Available online 27 October 2009

Keywords:
Methanol steam reforming
Cu/SiO_2
Modification of zinc oxide
Hydrogen production
Carbon monoxide
TPR
XRD
TEM
XPS
EXAFS

ABSTRACT

Methanol steam reforming to hydrogen and carbon dioxide is catalyzed over 30 wt% Cu/SiO_2 prepared by a sol–gel method. The addition of zinc ions to the starting material of the catalyst results in the suppression of CO formation in the reaction. Zinc oxide is highly dispersed in the catalyst even if the content is as high as 10 wt%. In the catalyst reduced with hydrogen, large Cu particles coexist with fine Cu particles which are oxidized to Cu_2O during the reaction. It is estimated that zinc oxide interacts with these Cu particles and stabilizes Cu^+ species formed during the reaction.

© 2009 Elsevier Inc. All rights reserved.

1. Introduction

Methanol is a potential feedstock of hydrogen processors for fuel cells especially for mobile applications such as electric vehicles because hydrogen can be easily produced by the steam reforming of methanol ($CH_3OH + H_2O \rightarrow 3H_2 + CO_2$) over copper catalysts at 200–300 °C [1]. Polymer electrolyte fuel cells (PEFCs) are generally employed for the portable devices by virtue of their compactness and mild operation conditions. However, the hydrogen fuel must not contain carbon monoxide above 10 ppm due to the poisoning of the catalytic anode [2]. Although the methanol steam reforming is fairly selective, by-production of carbon monoxide is not negligible over copper catalysts such as $Cu/ZnO/Al_2O_3$ and additional reactors are required in the fuel processor system for the removal of by-produced carbon monoxide [3]. Selective oxidation of carbon monoxide is often carried out to remove carbon monoxide to a level less than 10 ppm [2], but an excessive amount of oxygen is required in the process and it consumes hydrogen. Thus, suppression of CO by-production in methanol steam reforming is important to increase the efficiency of the hydrogen processors.

We have investigated a silica-supported copper catalyst prepared by the sol–gel method [4]. The CO selectivity is significantly lower than a commercial $Cu/ZnO/Al_2O_3$ in the reaction at 250 °C. This is probably because Cu^+ species is stabilized by the interaction with the silica support under the reaction condition; nevertheless, the selectivity increases at 300 °C to the same level as $Cu/ZnO/Al_2O_3$. In order to improve the performance of the Cu/SiO_2 catalyst, we have modified zinc oxide to it and mainly tested the activity to methanol steam reforming at 300 °C. It was reported that addition of zinc oxide to a Cu/SiO_2 catalyst increases the activity to methanol synthesis from carbon dioxide and hydrogen [5]. Here, it is shown that the CO selectivity decreases significantly by the modification of zinc oxide.

2. Experimental

A silica-supported copper catalyst (Cu/SiO_2) was prepared by the hydrolysis and polymerization of a mixture of tetramethoxy silane (Tokyo Chemical Industry), copper nitrate (Wako, S-grade), water, and methanol at room temperature for 1 day. After drying in air at 120 °C it was heated in air for 5 h at 500 °C for removal of NO_3^- anions and residual organic compounds. Zinc was introduced to Cu/SiO_2 by the addition of zinc nitrate (Wako, S-grade) to the starting materials. The catalysts (n-$ZnO/Cu/SiO_2$,

---

[*] Corresponding author. Fax: +81 72 751 9623.
E-mail address: yasu-matsumura@aist.go.jp (Y. Matsumura).

0021-9517/$ - see front matter © 2009 Elsevier Inc. All rights reserved.
doi:10.1016/j.jcat.2009.09.026

n represents the ZnO content in wt%) were also heated in air for 5 h at 500 °C. The Cu content was fixed at 30 wt% in the reduced form because Cu/SiO_2 with this content produced fairly low CO selectivity at 300 °C [4]. A commercial Cu/ZnO/Al_2O_3 catalyst (Süd-Chemie, MDC-3) was used as a reference. The catalyst was reported to be durable in the methanol steam reforming at 350 °C [6].

Catalytic tests were performed in a fixed-bed continuous-flow reactor operated under atmospheric pressure. A catalyst (0.50 g, granules of 10–20 mesh) was usually placed in a tube reactor made of stainless steel (i.d., 7 mm) with quartz wool plugs. After the pre-reduction in a stream of 15-vol% hydrogen diluted with argon (3.5 $dm^3 h^{-1}$) at 250 °C or 300 °C for 1 h, a mixture of methanol, steam, and argon (1.0/1.5/1.0 in molar ratio) was introduced with a flow rate of 10.6 $dm^3 h^{-1}$ at the same temperature as in the reduction. The effluent gas was dried with a cold trap at ca. −50 °C, and analyzed with an on-stream gas chromatograph (Shimadzu GC-8A; activated carbon, 2 m; Ar carrier) equipped with a thermal conductivity detector (TCD). The methanol conversion was determined from the material balance of the reactant and the products, and the error was within 5%. No formation of formaldehyde, methane, or methyl formate was observed.

Temperature-programed reduction (TPR) of the catalyst (0.50 g) was carried out in a stream of 15-vol% hydrogen diluted with argon at a flow rate of 3.5 $dm^3 h^{-1}$. Temperature of the sample bed was risen linearly at a rate of 200 °C h^{-1}. The hydrogen consumption was monitored by analyzing the hydrogen concentration with the on-stream GC every 3 min. No complete hydrogen consumption was observed in the reduction.

Powder XRD (X-ray diffraction) patterns of the catalysts were recorded in air at room temperature with an MAC Science MP6XCE diffractometer using nickel-filtered Cu Kα radiation. The Rietveld refinement of the patterns was carried out using the Rietveld software RIETAN-2000 [7]. To obtain the quantitative phase abundance, the XRD data of 30–70° in two theta were modeled with monoclinic CuO (space group, C2/c) and cubic Cu (Fm-3 m) using a pseudo-Voigt function. The factor of R_{wp} was always less than 5%.

The BET surface areas of the catalysts were determined from the isotherms of nitrogen physisorption.

The structure of 10-ZnO/Cu/SiO_2 after reduction with hydrogen at 250 °C for 1 h was evaluated by transmission electron microscopy (TEM) and high-angle annular dark field imaging in scanning transmission electron microscopy (HAADF/STEM) with energy dispersed X-ray Spectroscopic (EDS) analysis using an FEI Tecnai G^2 F20 Twin with an EDX detecting unit (EDAX Inc.) at the acceleration voltage of 200 kV. The sample was introduced to the microscope at room temperature in air.

X-ray photoelectron spectra (XPS) were recorded at room temperature with a JEOL JPS-9010MX spectrometer (Mg Kα). The catalysts used in the reaction were taken out from the reactor after cooling under an argon stream for 12 h or longer and mounted in air to a sample holder. A sample reduced with hydrogen at 250 °C for 1 h was mounted to a sample holder under Ar atmosphere and measured in situ. Binding energies were corrected by the reference of the C 1s line at 284.6 eV. The surface atomic concentrations of Cu, Zn, Si, and O were calculated from the peak areas using the atomic relative sensitivity factors (ARSF) of Cu $2p_{3/2}$ (13), Zn $2p_{3/2}$ (17), Si 2p (1.0), and O 1s (2.4) determined by measuring standard materials of copper and zinc plates, silicon wafer, and quartz glass plate. The concentration analysis using ARSF is quantitative and the uncertainty is less than 2% [8].

The profile of EXAFS (extended X-ray absorption fine structure) for 10-ZnO/Cu/SiO_2 reduced with hydrogen at 250 °C for 1 h was taken at room temperature in transmission mode for Zn K-edge at beam-line BL14B2 of SPring-8. The sample was handled in air and vacuum-sealed with polyethylene films. The Fourier transformation was performed on k^3-weighted EXAFS oscillations in the range of 30–150 nm^{-1}. The analysis was performed with a program of "REX2000" supplied by Rigaku.

The surface of the catalyst reduced with hydrogen at 250 °C for 1 h was oxidized by the decomposition of N_2O at 50 °C [9]. The amount of N_2 produced was measured with a TCD.

3. Results

3.1. Methanol steam reforming over ZnO-modified Cu/SiO_2

Steam reforming of methanol was carried out over the copper catalysts. Hydrogen and carbon dioxide were almost selectively produced at 300 °C. Addition of zinc oxide significantly lessened the CO selectivity of Cu/SiO_2 and discernibly increased the catalytic activity. The activities at 6 h-on-stream are shown in Fig. 1. When double the amount of Cu/SiO_2 (1.0 g) was charged in the reactor, the CO selectivity increased to 2.5% with 88% methanol conversion at 300 °C. The CO selectivity leveled off at the ZnO content of 5 wt%. The activities at 250 °C were mostly parallel to those at 300 °C and the CO selectivity decreased by the addition of zinc oxide. The activity of 5-ZnO/Cu/SiO_2 at 300 °C was almost stable within 6 h-on-stream, and the CO selectivity was about a half of that with Cu/ZnO/Al_2O_3 (Fig. 2). When the amount of 5-ZnO/Cu/SiO_2 was

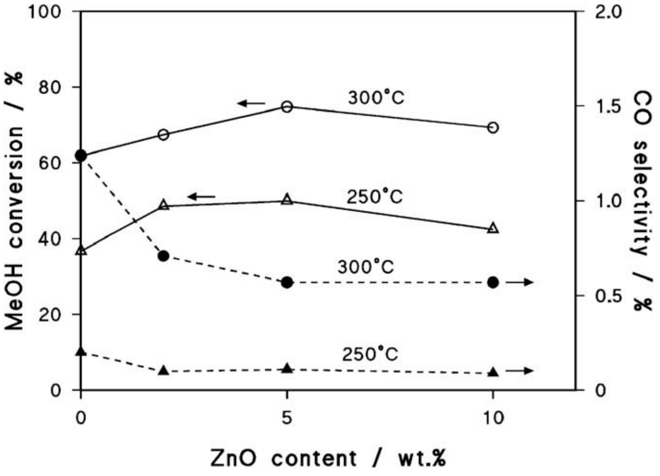

Fig. 1. Catalytic activity of Cu/SiO_2 and ZnO/Cu/SiO_2 in methanol steam reforming after 6 h.

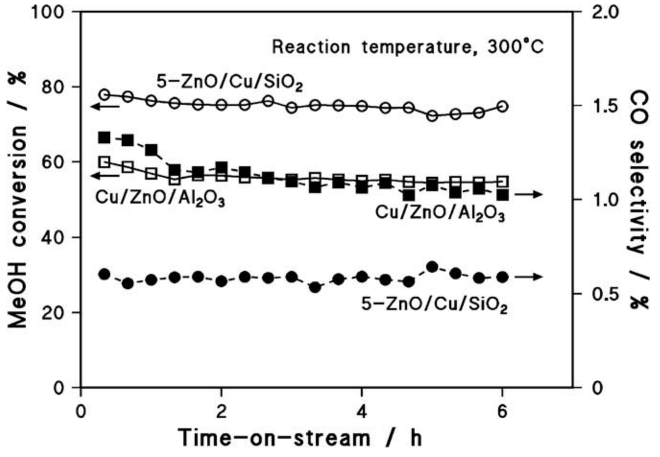

Fig. 2. Comparison of the catalytic activity of 5-ZnO/Cu/SiO_2 to that of a commercial Cu/ZnO/Al_2O_3 at 300 °C.

1.0 g, the CO selectivity was increased to 1.0% with 100% methanol conversion at 300 °C.

3.2. TPR of copper catalysts

Reduction of the copper catalysts started at ca. 150 °C in TPR experiments regardless of the ZnO content (Fig. 3). Two peaks were distinguished in the profile of Cu/SiO_2. The peaks seemed to merge in the profile for $ZnO/Cu/SiO_2$. However, the shape of the profile showed the presence of a shoulder peak and the profile can be deconvoluted into two Gaussian peaks (Table 1). The molar amounts of hydrogen consumption corresponded with the Cu content in the catalysts (4.7 mmol g^{-1}), showing complete reduction of CuO in the catalysts. In a TPR experiment, Cu/SiO_2 was reduced up to 210 °C and quenched under an argon stream. The H_2 consumption was 2.2 mmol g^{-1}. In the case of 10-$ZnO/Cu/SiO_2$ reduced up to 210 °C, the H_2 consumption was 3.7 mmol g^{-1}.

3.3. XRD patterns for copper catalysts

Only the XRD peaks attributed to CuO were recorded in the pattern of Cu/SiO_2 as prepared (Fig. 4a) [10]. The mean crystallite size of CuO was determined as 24 nm from the line broadening of the peak at 48.8° in 2θ using Scherrer equation [11]. Small peaks at 43.4° and 50.5° being assigned to Cu(1 1 1) and Cu(200) [10], respectively, appeared with the peaks for CuO in the XRD pattern of Cu/SiO_2 reduced up to 210 °C in the TPR (Fig. 4b). The mean crystallite size of Cu was 34 nm from the line broadening of Cu(1 1 1) and the size of CuO was 26 nm. The molar fraction of Cu/(Cu + CuO) determined by the Rietveld analysis was 33%. The peaks for CuO were completely diminished by the reduction at 250 °C for 1 h and the crystallite size of Cu was 34 nm (Fig. 4c).

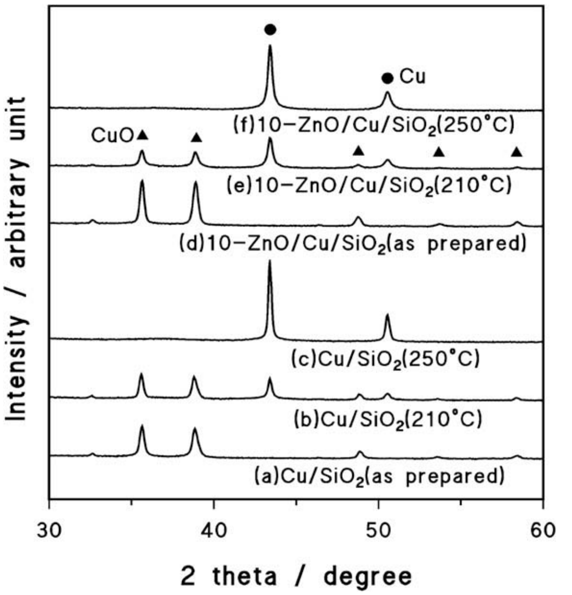

Fig. 4. XRD patterns of Cu/SiO_2 and 10-$ZnO/Cu/SiO_2$. (a) Cu/SiO_2 as prepared, (b) reduced with hydrogen up to 210 °C, (c) reduced at 250 °C, (d) 10-$ZnO/Cu/SiO_2$ as prepared, (e) reduced up to 210 °C, and (f) reduced at 250 °C.

The XRD pattern for 10-$ZnO/Cu/SiO_2$ as prepared was similar to that of Cu/SiO_2 (Fig. 4d), and the mean crystallite size of CuO was 21 nm. The XRD peaks for Cu metal appeared with those for CuO in the pattern of the sample reduced up to 210 °C (Fig. 4e). The mean crystallite sizes of Cu and CuO were 25 nm and 23 nm, respectively. The molar fractions of Cu/(Cu + CuO) determined by

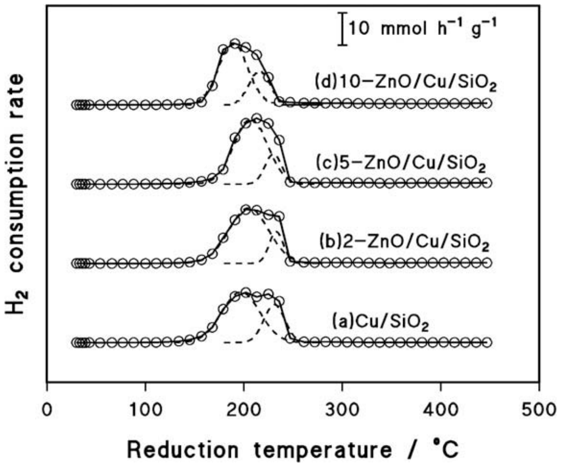

Fig. 3. Profiles of TPR for Cu/SiO_2 and $ZnO/Cu/SiO_2$ with a heating rate of 200 °C h^{-1}.

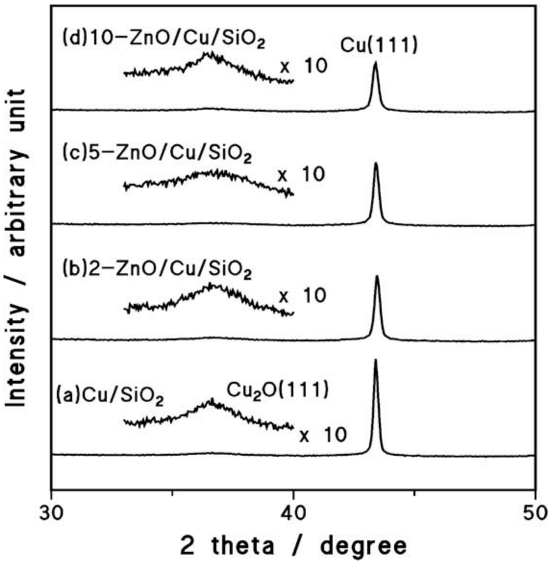

Fig. 5. XRD patterns of Cu/SiO_2 and $ZnO/Cu/SiO_2$ after the reaction at 300 °C for 6 h. (a) Cu/SiO_2, (b) 2-$ZnO/Cu/SiO_2$, (c) 5-$ZnO/Cu/SiO_2$, and (d) 10-$ZnO/Cu/SiO_2$.

Table 1
The amounts of hydrogen consumption in the TPR experiment.

Catalyst	Peak 1		Peak 2	
	Temperature (°C)	H_2 consumption (mmol g^{-1})	Temperature (°C)	H_2 consumption (mmol g^{-1})
Cu/SiO_2	197	3.2	231	1.5
2-$ZnO/Cu/SiO_2$	205	3.7	233	0.8
5-$ZnO/Cu/SiO_2$	207	3.8	230	0.9
10-$ZnO/Cu/SiO_2$	185	3.2	212	1.3

the Rietveld analysis was 53%. Only the peaks attributed to Cu metal were recorded in the XRD pattern for the sample reduced at 250 °C for 1 h (Fig. 4f). The mean crystallite size of Cu was 25 nm.

A broad peak at 36.7° assigned to Cu_2O (1 1 1) was recorded with the peaks for Cu metal in the XRD pattern of Cu/SiO_2 after the reaction at 300 °C for 6 h (Fig. 5a) [10]. Addition of zinc oxide to Cu/SiO_2 resulted in a discernible line broadening of the peak at 43.4° attributed to Cu metal (Figs. 5b–d). The mean crystallite size of Cu metal for Cu/SiO_2 was 39 nm, and it was decreased to 29–33 nm by the addition of zinc oxide (Table 2). No significant change in the weak peak for Cu_2O was observed by the addition. The mean crystallite size was 3–4 nm regardless of the samples.

Table 2
Mean crystallite sizes and BET surface areas of the catalysts after methanol steam reforming at 300 °C for 6 h.

Catalyst	Crystallite size (nm)		BET surface area ($m^2\ g^{-1}$)
	Cu_2O	Cu	
Cu/SiO_2	4	39	291
Cu/SiO_2[a]	–	34	360
2-ZnO/Cu/SiO_2	4	33	273
5-ZnO/Cu/SiO_2	3	33	239
10-ZnO/Cu/SiO_2	4	29	244
10-ZnO/Cu/SiO_2[a]	–	25	277

[a] Just after reduction with hydrogen at 250 °C for 1 h.

3.4. TEM and HAADF/STEM of ZnO-modified Cu/SiO_2

Dark portions were seen in a TEM image of an aggregate of 10-ZnO/Cu/SiO_2 (Fig. 6a), while the edges of the aggregate were in the amorphous shape (Fig. 6b). In the HAADF/STEM image which shows the same area as in Fig. 6a, bright and round particles with the size of 11–13 nm were mainly present (Fig. 6c), while some particles seemed to bond. Since the intensity of the HAADF/STEM image relates to the square of atomic number of the detected atoms, i.e., Z^2, the bright grains should consist of copper. This is supported by the EDX analysis (Fig. 6d); Cu was mainly detected at the bright points 1–3 by EDS analysis and Si was mainly present at the dark points 4 and 5 (Fig. 6d). Zinc was also detected with Cu at the points 2 and 3, but no particles were identified as zinc oxide. In the amorphous portion (Fig. 7a), small and dark spots with the size of ca. 1 nm were seen (some spots are indicated with arrows in Fig. 7b). The HAADF/STEM image (Fig. 7c) was obtained at a higher sensitivity than that for Fig. 6c. In an amorphous portion, Si was mainly present while Cu and Zn were also detected (Fig. 7d).

3.5. XPS of the copper catalysts

The surfaces of Cu/SiO_2 and ZnO/Cu/SiO_2 after the reaction at 300 °C were characterized by XPS. The binding energies of Cu $2p_{3/2}$ were 931.6–932.6 eV (Fig. 8), whereas the energies for Cu metal and Cu_2O were 932.7 and 932.4 eV, respectively [12]. In order to identify the electronic state, the Auger line of Cu L_3VV was recorded and the kinetic energies were 917.0–918.0 eV (Fig. 9).

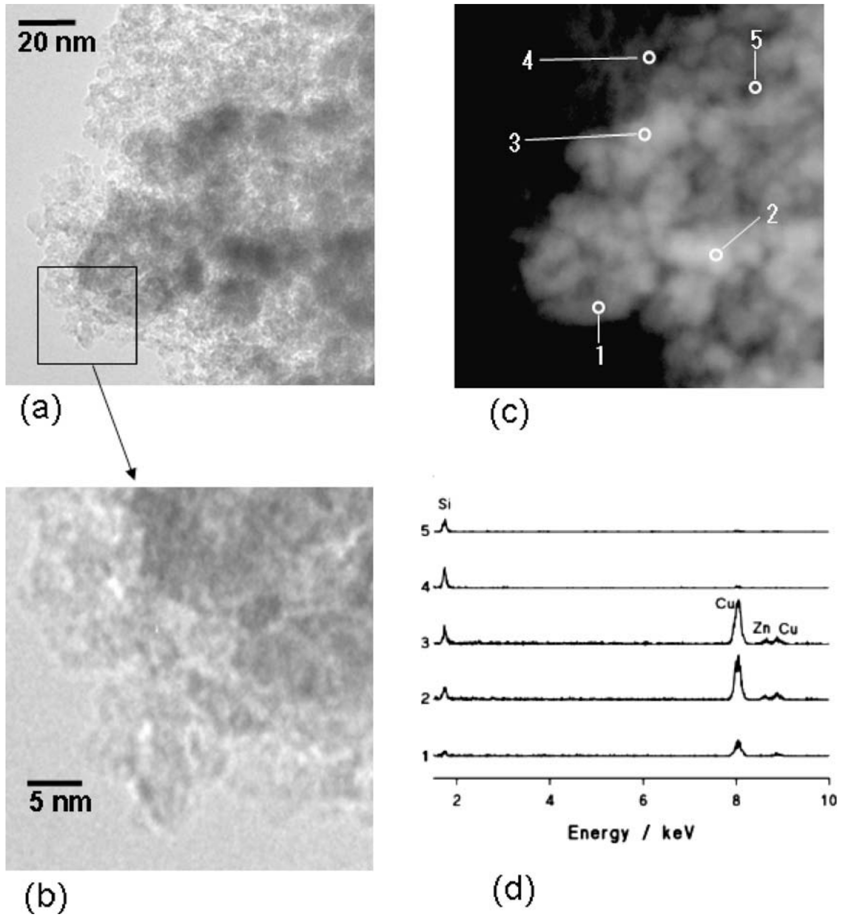

Fig. 6. TEM and HAADF/STEM images and EDS analysis of 10-ZnO/Cu/SiO_2 reduced with hydrogen at 250 °C for 1 h. (a) TEM image, (b) partial enlargement of the TEM image, (c) HAADF/STEM image, and (d) EDS spectra on points 1–5.

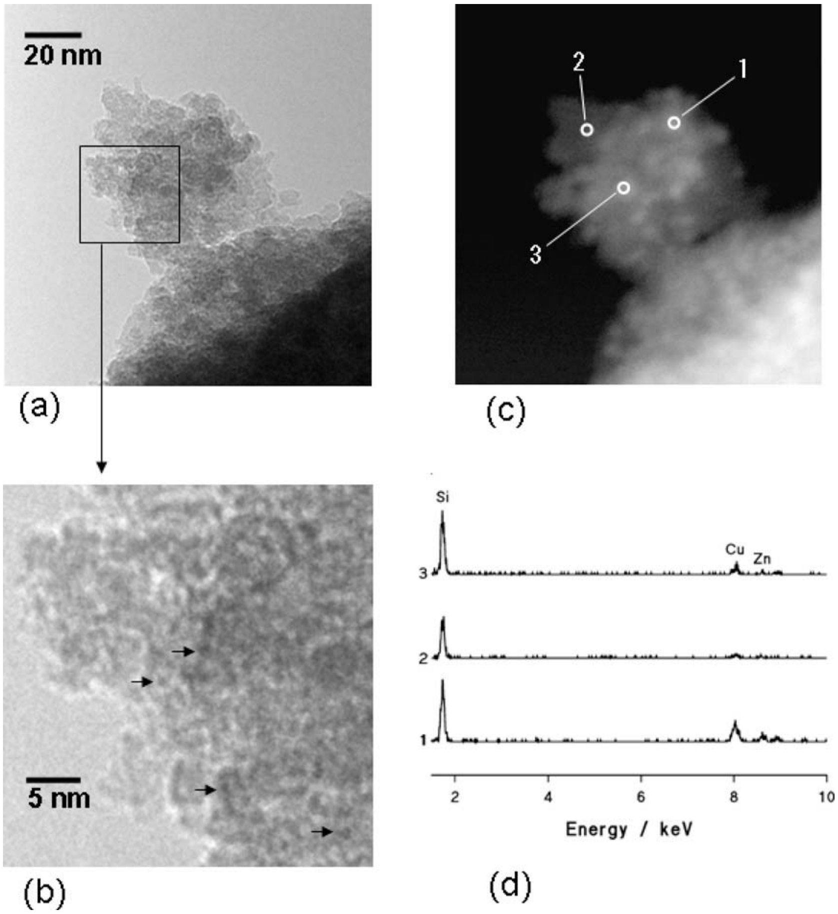

Fig. 7. TEM and HAADF/STEM images and EDS analysis of amorphous portion in 10-ZnO/Cu/SiO_2 reduced with hydrogen at 250 °C for 1 h. (a) TEM image, (b) partial enlargement of the TEM image, (c) HAADF/STEM image, and (d) EDS spectra on points 1–3.

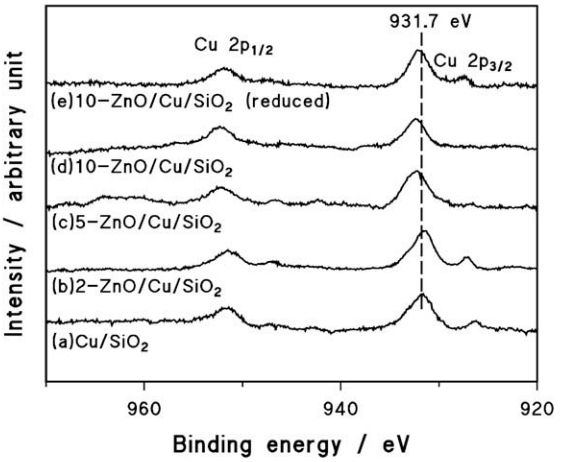

Fig. 8. XPS of Cu 2p region for Cu/SiO_2 and ZnO/Cu/SiO_2 after the reaction at 300 °C for 6 h. (a) Cu/SiO_2, (b) 2-ZnO/Cu/SiO_2, (c) 5-ZnO/Cu/SiO_2, (d) 10-ZnO/Cu/SiO_2, and (e) 10-ZnO/Cu/SiO_2 reduced with hydrogen at 300 °C for 1 h.

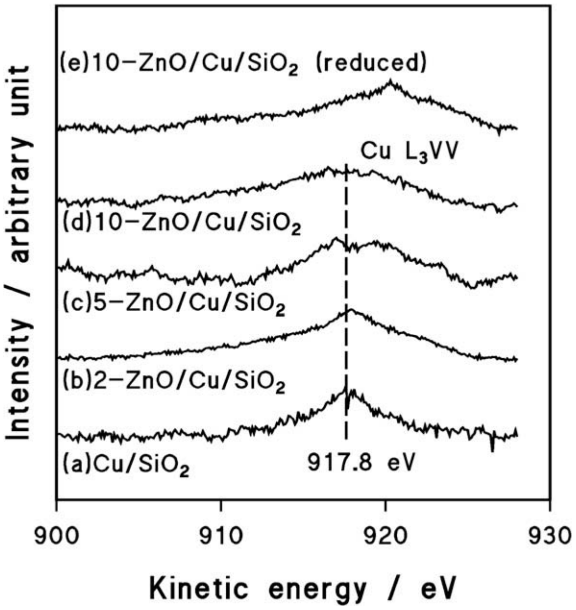

Fig. 9. Auger line of Cu L_3VV for Cu/SiO_2 and ZnO/Cu/SiO_2 after the reaction at 300 °C for 6 h. (a) Cu/SiO_2, (b) 2-ZnO/Cu/SiO_2, (c) 5-ZnO/Cu/SiO_2, (d) 10-ZnO/Cu/SiO_2, and (e) 10-ZnO/Cu/SiO_2 reduced with hydrogen at 300 °C for 1 h.

The energies for Cu metal and Cu_2O are 917.8 and 916.8 eV, respectively. The α values (Auger parameter + photon energy) were 1849.5–1850.0 eV being close to 1849.4 eV for Cu_2O (Table 3) [12]. The value for the metallic Cu is 1851.3 eV [12].

The α values of Cu/SiO_2 and 10-ZnO/CuSiO_2 reduced at 250 °C with hydrogen were both 1850.3 eV where the samples were handled in situ (see Table 3). Although 10-ZnO/Cu/SiO_2 reduced with hydrogen at 300 °C for 1 h was handled in air, the α value was 1850.5 eV, showing that the handling in air did not affect the XPS measurement seriously.

The binding energies of Zn $2p_{3/2}$ for the samples containing zinc were 1022.7 ± 0.2 eV (Fig. 10), and the energies of O 1s and Si 2p were 533.0 ± 0.2 eV and 103.3 ± 0.1 eV, respectively, regardless of the samples. The surface atomic concentrations of Cu, Zn, and Si are also given in Table 3.

3.6. BET surface area of the catalyst after reaction

The BET surface area of Cu/SiO_2 after the reaction at 300 °C was 291 $m^2\,g^{-1}$ and it was decreased to 239–273 $m^2\,g^{-1}$ by the addition of zinc oxide (see Table 2). The areas of Cu/SiO_2 and 10-$ZnO/Cu/SiO_2$ just after the reduction with hydrogen at 250 °C for 1 h were 360 $m^2\,g^{-1}$ and 277 $m^2\,g^{-1}$, respectively.

3.7. Structural analyses of zinc in ZnO-modified Cu/SiO_2 by EXAFS

In order to analyze the atomic structure of zinc, EXAFS (extended X-ray absorption fine structure) analysis was performed for 10-$ZnO/Cu/SiO_2$ reduced at 250 °C for 1 h. The Fourier transform showed the presence of a peak at 0.16 nm (phase shift uncorrected) attributed to Zn–O interaction (Fig. 11). The distance was slightly shorter than that of a ZnO standard sample, but no peak attributed to Zn–Zn interaction was present in the profile for 10-$ZnO/Cu/SiO_2$.

3.8. Surface oxidation of ZnO-modified Cu/SiO_2 with N_2O

The surface amounts of copper on Cu/SiO_2 and 10-$ZnO/Cu/SiO_2$ reduced with hydrogen at 250 °C were evaluated by the surface oxidation with N_2O. The quantities of N_2O decomposed were 0.039 mmol g^{-1} and 0.049 mmol g^{-1}, respectively. The Cu surface amounts were 0.078 mmol g^{-1} and 0.098 mmol g^{-1}, respectively, on the basis of the stoichiometry, that is, $2Cu + N_2O \rightarrow Cu_2O + N_2$ [9].

4. Discussion

4.1. Morphology of ZnO-modified Cu/SiO_2

The XRD pattern of Cu/SiO_2 reduced with hydrogen at 250 °C shows the presence of large Cu particles with the mean crystallite size of 34 nm. In the TPR of Cu/SiO_2 up to 210 °C, 48% of CuO in the sample is reduced, but the reducibility of the large CuO particles determined by XRD (33%) is considerably smaller than that. This is probably due to the co-existence of fine CuO particles that are undetectable by XRD, as discussed in the previous paper [4]. A single TPR peak at around 190 °C was observed with 10 wt% Cu/SiO_2 containing fine CuO particles only [4], suggesting that the first peak is not due to reduction of Cu^{2+} to Cu^{+}. Hence, the TPR peak deconvoluted at the lower temperature (peak 1) and it can be attributed to the reduction of the fine CuO particles (see Table 1).

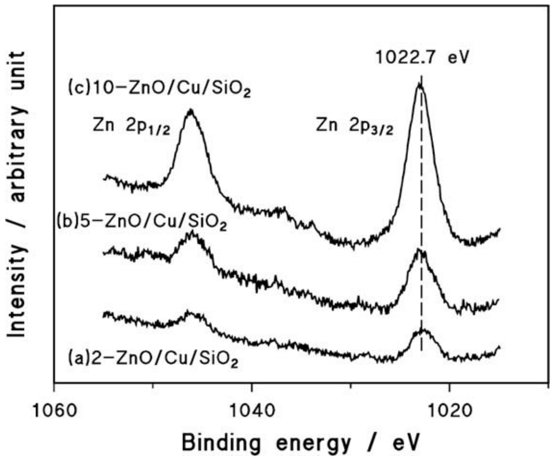

Fig. 10. XPS of Zn 2p region for $ZnO/Cu/SiO_2$ after the reaction at 300 °C for 6 h. (a) 2-$ZnO/Cu/SiO_2$, (b) 5-$ZnO/Cu/SiO_2$, and (c) 10-$ZnO/Cu/SiO_2$.

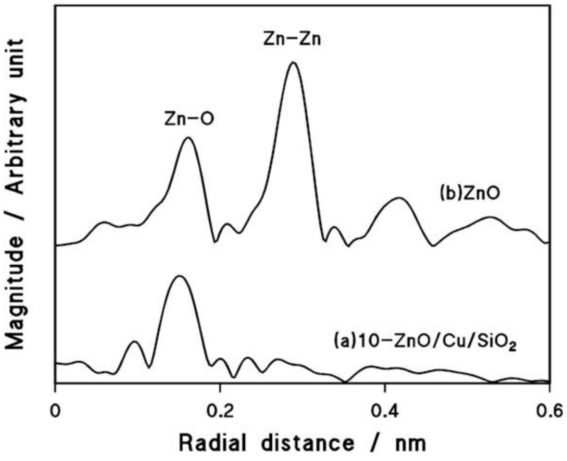

Fig. 11. Fourier transforms of k^3-weighted Zn K-edge EXAFS for (a) 10-$ZnO/Cu/SiO_2$ reduced with hydrogen at 250 °C for 1 h and (b) ZnO.

While the TPR peaks for 10-$ZnO/Cu/SiO_2$ are not separated clearly (see Fig. 3d), the reducibility up to 210 °C is evaluated as 82% by TPR and significantly higher than the reducibility determined by XRD (53%). Hence, the fine CuO particles undetectable by XRD should be also present in the unreduced sample and they must be responsible for the peak 1 in the TPR (see Table 1). Actually, copper is detected in the amorphous portion mainly comprised of silica despite the lack of presence of large Cu particles in the TEM and STEM (see Fig. 7). The dark spots with the size of

Table 3
Summary of the XPS data for the catalysts after methanol steam reforming at 300 °C for 6 h.

Catalyst	Cu $2p_{3/2}$ (eV)	Cu L_3VV (eV)	α (eV)	Surface atomic composition (%)		
				Cu	Zn	Si
Cu/SiO_2	931.7	917.8	1849.5	5	0	28
Cu/SiO_2[a]	932.5	917.8	1850.3	2	0	28
2-$ZnO/Cu/SiO_2$	931.6	918.0	1849.6	6	1	27
5-$ZnO/Cu/SiO_2$	932.6	917.0	1849.6	7	2	18
10-$ZnO/Cu/SiO_2$	932.4	917.6	1850.0	4	6	17
10-$ZnO/Cu/SiO_2$[a]	932.3	918.0	1850.3	2	3	28
10-$ZnO/Cu/SiO_2$[b]	932.1	918.4	1850.5	4	6	29

[a] Just after reduction with hydrogen at 250 °C for 1 h (in situ).
[b] Just after reduction with hydrogen at 300 °C for 1 h (ex situ).

ca. 1 nm in Fig. 7b may be the fine Cu particles because the silica particle with this size is less distinguishable with TEM.

Since the H_2 consumption in the TPR corresponds well with the Cu content of the catalyst, the quantity of the fine Cu particles is estimated from the H_2 consumption for the peak 1 (see Table 1). Assuming that the fine particles in 10-ZnO/Cu/SiO_2 reduced at 250 °C are spherical with a diameter of 1 nm and that all the particles are on the surface, the Cu surface amount of the fine particles is estimated to be 7 mmol g^{-1} (Table 4); here, the site density of Cu is 0.032 mmol m^{-2} on the basis of the atomic radius. The amount largely exceeds that determined by the N_2O adsorption (0.078 mmol g^{-1}), showing that the major part of the fine particles is buried in the support. In the cases of silica-supported catalysts prepared by the sol–gel technique, the major part of metallic particles is often encapsulated in the support [13,14]. The surface of metallic copper catalysts is often oxidized to Cu^{2+} in air [15], but no such oxidation takes place with Cu/SiO_2 and ZnO/Cu/SiO_2 presumably because of the encapsulation in the silica support. Silicon is always detected in the EDS analysis on the surface of 10-ZnO/Cu/SiO_2 (see Figs. 6d and 7d), indicating that most of the Cu particles are covered with the silica support. Although Cu particles sinter easily at high temperatures, the surface Cu concentration of 10-ZnO/Cu/SiO_2 after the reduction at 300 °C is significantly higher than that after the reduction at 250 °C (see Table 3). Hence, a part of the fine Cu particles encapsulated in the support is supposed to come out of the support in the process of reduction at 300 °C.

No peaks attributed to zinc oxide are present in the XRD patterns of ZnO/Cu/SiO_2 (see Figs. 4 and 5). The Fourier transform of the EXAFS for 10-ZnO/Cu/SiO_2 shows lack of Zn–Zn interaction (see Fig. 11a). The spectrum is very similar to that for ZnO/SiO_2 prepared by a sol–gel method and can be assigned as zinc oxide species such as oligomers/clusters consisting of ZnO_4 tetrahedra [16]. The binding energy of Zn $2p_{3/2}$ for ZnO/Cu/SiO_2 is significantly higher than those for ZnO (1022.1 eV) and Zn_2SiO_4 (1021.7 eV) [11]. Since the binding energy usually depends on the valence, the zinc ions in ZnO/Cu/SiO_2 should be electron-deficient in comparison with those in ZnO and it probably reflects the local structure of the zinc oxide species.

The amount of surface Cu atoms on the catalyst can be roughly estimated from the BET surface area and the surface atomic composition determined by XPS, assuming the site densities of Cu^+ as 0.058 mmol m^{-2}, Zn^{2+} as 0.077 mmol m^{-2}, Si^{4+} as 0.35 mmol m^{-2}, and O^{2-} as 0.030 mmol m^{-2} on the basis of the ionic radii [4]. Both the values for Cu/SiO_2 and 10-ZnO/Cu/SiO_2 reduced with hydrogen at 250 °C for 1 h are calculated as 0.2 mmol g^{-1} (see Table 4). Since the amounts determined by the N_2O adsorption are 0.078 mmol g^{-1} and 0.098 mmol g^{-1}, respectively, the values obtained from BET and XPS are probably overestimated.

Table 4

Estimation of Cu surface amount of the catalysts after methanol steam reforming at 300 °C for 6 h.

Catalyst	Cu surface amount[a] (mmol g^{-1})	Cu amount on particle surface[b] (mmol g^{-1})	
	Cu	Fine	Large
Cu/SiO_2	0.6	2	0.05
Cu/SiO_2[c]	0.2	–	0.06
2-ZnO/Cu/SiO_2	0.7	2	0.04
5-ZnO/Cu/SiO_2	0.6	3	0.04
10-ZnO/Cu/SiO_2	0.4	2	0.07
10-ZnO/Cu/SiO_2[c]	0.2	7[d]	0.08

[a] Evaluated from the surface atomic concentrations and BET surface area.
[b] Evaluated from the crystallite size in Table 2 and the quantity in Table 1.
[c] Just after reduction with hydrogen at 250 °C for 1 h.
[d] The particle size is assumed to be 1 nm.

4.2. Effect of ZnO on the catalytic performance of Cu/SiO_2

The presence of Cu_2O is detected in the XRD patterns for Cu/SiO_2 and ZnO/Cu/SiO_2 after the reaction at 300 °C (see Fig. 5). Since no peak attributed to Cu_2O is present in the patterns for the samples after the reduction with hydrogen at 250 °C (see Fig. 4), the formation of Cu_2O is not due to the handling of the samples in air. That is, the Cu_2O species are formed during the reaction. The small crystallite size strongly suggests partial oxidation of the fine Cu particles undetectable by XRD (see Table 2).

The quantity of the large Cu particles can be estimated from the H_2 consumption for the peak 2 in TPR (see Table 1). Assuming that all the large Cu particles in Cu/SiO_2 are spherical with a diameter of 39 nm and all the particles are on the surface, the Cu surface amount on the large Cu particles will be 0.05 mmol g^{-1} (see Table 4). On the other hand, the Cu surface amount of Cu/SiO_2 after the reaction is calculated as 0.6 mmol g^{-1} (see Table 4). The amount is evaluated from the BET surface area and the surface atomic concentrations because the formation of Cu_2O during the reaction prevents correct evaluation using N_2O adsorption. The Cu surface amount overwhelms the amount on the large particles, even if the former amount determined from BET and XPS is overestimated. Thus, the Cu atoms on the large particles are minor species and the information of the Cu $2p_{3/2}$ and Cu L_3VV in the XPS for the catalyst after the reaction is considered to originate mainly from the fine particles. As can be seen in Fig. 6c, the shape and the size of the large Cu particles are not uniform. The mean crystallite size of 10-ZnO/Cu/SiO_2 reduced at 250 °C is 25 nm. On the other hand, the main particle size observed in Fig. 6c is a half of the mean crystallite size, while some particles seem to bond together. If the particle size of Cu/SiO_2 is a half of the crystallite size, the Cu surface amount on the large particles will be 0.10 mmol g^{-1}. The value is still small in comparison with the Cu surface amount. In addition, the actual surface amount of the large particles is supposed to be considerably lower than the estimated value because the majority of the large particles are probably encapsulated in the support.

Since the α value obtained from the XPS suggests that the major surface species are present as Cu^+ (see Table 3), the fine Cu particles are oxidized to Cu_2O during the reaction. This is in harmony with the observation from the XRD measurement. In the cases of 2-ZnO/Cu/SiO_2 and 5-ZnO/Cu/SiO_2 the Cu surface amounts also overwhelm those for the large Cu particles (see Table 4), suggesting that the Cu atoms on the large particles are minor species.

Carbon monoxide is considered as a secondary product of the steam reforming of methanol over Cu/ZnO/Al_2O_3 by the reverse water gas-shift (WGS) reaction ($CO_2 + H_2 \rightarrow CO + H_2O$) [17,18]. In this mechanism CO production is enhanced at a high methanol conversion. The CO selectivity with Cu/SiO_2 increased from 1.2% to 2.5% at a low space velocity at 300 °C, where the conversion also increased from 62% to 88%. In the case of 5-ZnO/Cu/SiO_2, the selectivity of 0.6% at the conversion of 75% increased to 1.0% at the 100% conversion. Decomposition of methanol is a possible mechanism of CO by-production [19–21], but the CO selectivity will be independent of the conversion. Hence, it is estimated that the CO formation on Cu/SiO_2 and ZnO/Cu/SiO_2 is mainly caused by the reverse WGS reaction.

A mechanism for the reverse WGS has been proposed on copper catalysts, that is, $CO_2 + 2Cu \rightarrow CO + Cu_2O$ and $H_2 + Cu_2O \rightarrow H_2O + 2Cu$ [22], indicating that stabilization of Cu^+ species such as Cu_2O suppresses the reverse WGS and causes low CO selectivity. Ritzkopf et al. reported that a zirconia-supported copper catalyst gives low selectivity to carbon monoxide in methanol steam reforming and the copper surface is oxidized to Cu^+ state during the reaction [23]. Hence, Cu/SiO_2 is advantageous in CO suppression because Cu^+ species are dominant on the surface [4]. The CO selectivity of Cu/SiO_2 decreases significantly by addition of zinc oxide as small as 2 wt% despite an increase in the methanol conversion (see Fig. 1), suggesting that the reverse WGS is suppressed by the addition of zinc oxide. The CO selectivity with Cu/SiO_2 at the conversion of 75% is expected to be ca. 2%. The selectivity with $5\text{-}ZnO/Cu/SiO_2$ is only 0.6% at the same conversion, showing that the addition of ZnO to Cu/SiO_2 is effective for the suppression of CO by-production at 300 °C.

Since the addition of zinc oxide to the catalyst does not greatly change the properties of copper particles as shown in Figs. 3, 5 and 8, the basic properties of the active sites remain after the ZnO modification. Nakamura et al. showed that co-existence of zinc oxide with silica-supported copper increases oxygen coverage of copper surface, suggesting formation of $Cu^{+}{-}O{-}Zn^{2+}$ species [24,25]. Peak broadening in the Auger line of Cu L_3VV is observed with the samples containing zinc oxide (see Fig. 9), and it is probably due to the interaction between the fine Cu particles and zinc oxide which is highly dispersed as evidenced by the EXAFS analysis (see Fig. 11). The EDS analysis on the portion of amorphous silica, where the fine Cu particles should be present, shows the presence of zinc with copper (see Fig. 7d). Thus, it is estimated that the interaction stabilizes Cu^{+} species during the reaction even at 300 °C and prevents CO formation from hydrogen and carbon dioxide.

The activity of the large Cu particles cannot be negligible as discussed in the previous paper [4], although the amount of Cu atoms exposed on the surface is estimated to be small. Since the Cu surface amount on the large particles is significantly smaller than that on the fine particles, the detection of the surface state of the large particles is difficult by XPS. However, the EDS analysis shows that Zn is present on the large Cu particles (e.g., points 2 and 3 in Fig. 6c). Hence, zinc oxide also modifies the surface of large Cu particles and may stabilize Cu^{+} species by forming $Cu^{+}{-}O{-}Zn^{2+}$ species [24,25]. Günter et al. reported that dissolution of zinc atoms up to 4 mol% in Cu lattice under the reduction of Cu/ZnO with hydrogen at 250 °C [26].

The methanol conversion with Cu/SiO_2 at 300 °C increases discernibly with the addition of zinc oxide up to 5 wt% (see Fig. 1). However, the turn-over frequencies (TOF) are calculated as $0.08\ s^{-1}$ for Cu/SiO_2, $0.07\ s^{-1}$ for $2\text{-}ZnO/Cu/SiO_2$, and $0.09\ s^{-1}$ for $5\text{-}ZnO/Cu/SiO_2$ on the basis of the quantity of methanol reacted and the Cu surface amount in Table 4. Since the conversions are in a narrow range (62–75%) where no saturation takes place, the catalytic activity relates approximately to the conversion. Thus, zinc oxide does not significantly activate the copper sites and the increase in the catalytic activity is probably caused by indirect effects of zinc oxide. In the case of $10\text{-}ZnO/Cu/SiO_2$ the TOF is $0.14\ s^{-1}$. Since the Cu surface amount of the large particles on $10\text{-}ZnO/Cu/SiO_2$ is appreciably high in comparison with the other catalysts (see Table 4), the larger contribution of the large Cu particles may increase the conversion [4].

5. Conclusions

Addition of zinc oxide to 30 wt% Cu/SiO_2 prepared by a sol–gel method significantly suppresses CO by-production in the steam reforming of methanol to hydrogen and carbon dioxide at 300 °C. Zinc oxide is highly dispersed in the catalyst and can be assigned as the species such as oligomers/clusters consisting of ZnO_4 tetrahedra. In the reduced form of Cu/SiO_2 modified/unmodified with zinc oxide, large Cu particles with the mean crystallite size at around 30 nm coexist with fine Cu particles which cannot be detected by XRD. The fine Cu particles are oxidized to Cu_2O during the reaction. The presence of zinc oxide probably stabilizes the Cu^{+} species on the surface and prevents the reduction to metallic Cu in the reaction. Zinc oxide is also present on the surface of the large Cu particles and may stabilize Cu^{+} species by forming $Cu^{+}{-}O{-}Zn^{2+}$ species. The presence of zinc oxide does not affect the activity of the Cu sites significantly.

References

[1] A. Qi, B. Peppley, K. Karan, Fuel Process. Technol. 88 (2007) 3.
[2] P. Marques, N.F.P. Ribeiro, M. Schmal, D.A.G. Aranda, M.M.V.M. Souza, J. Power Sources 158 (2006) 504.
[3] C. Song, in: N. Brandon, D. Thompsett (Eds.), Fuel Cells Compendium, Elsevier, Oxford, 2005, p. 53.
[4] Y. Matsumura, H. Ishibe, Appl. Catal. B 86 (2009) 114.
[5] E.K. Poels, D.S. Brands, Appl. Catal. A 191 (2000) 83.
[6] Y.-M. Lin, M.-H. Rei, Catal. Today 67 (2001) 77.
[7] F. Izumi, T. Ikeda, Mater. Sci. Forum 321–324 (2000) 198.
[8] ISO 18118, 2004.
[9] J.W. Evans, M.S. Wainright, A.J. Bridgewater, D.J. Young, Appl. Catal. 7 (1983) 75.
[10] JCPDS files, 40836, 50667, and 410254.
[11] C. Hammond, The Basics of Crystallography and Diffraction, Oxford University Press, New York, 1997.
[12] C.D. Wagner, in: D. Briggs, M.P. Seah (Eds.), Practical Surface Analysis, Auger and X-ray Photoelectron Spectroscopy, second ed., vol. 1, John Wiley & Sons, Inc., New York, 1990, p. 595.
[13] Z. Wang, Q. Liu, J. Yu, T. Wu, G. Wang, Appl. Catal. A 239 (2003) 87.
[14] Y. Matsumura, N. Tode, T. Yazawa, M. Haruta, J. Mol. Catal. A 99 (1995) 183.
[15] Y. Matsumura, H. Ishibe, Appl. Catal. B 91 (2009) 524.
[16] H. Yoshida, T. Shimizu, C. Murata, T. Hattori, J. Catal. 220 (2003) 226.
[17] J. Agrell, H. Birgersson, M. Boutonnet, J. Power Sources 106 (2002) 249.
[18] H. Purnama, T. Ressler, R.E. Jentoft, H. Soerijanto, R. Schlögl, R. Schomäcker, Appl. Catal. A 259 (2004) 83.
[19] Y. Choi, H.G. Stenger, Appl. Catal. B 38 (2002) 259.
[20] B.A. Peppley, J.C. Amphlett, L.M. Kearns, R.F. Mann, Appl. Catal. A 179 (1999) 21.
[21] A. Mastalir, B. Frank, A. Szizybalski, H. Soerijanto, A. Deshpande, M. Niederberger, R. Schomäcker, R. Schlögl, T. Ressler, J. Catal. 230 (2005) 464.
[22] M.J.L. Ginés, A.J. Marchi, C.R. Apesteguía, Appl. Catal. A 154 (1997) 155.
[23] I. Ritzkopf, S. Vukojević, C. Weidenthaler, J.-D. Grunwaldt, F. Schüth, Appl. Catal. A 302 (2006) 215.
[24] J. Nakamura, T. Uchijima, Y. Kanai, T. Fujitani, Catal. Today 28 (1996) 223.
[25] I. Nakamura, T. Fujitani, T. Uchijima, J. Nakamura, Surf. Sci. 400 (1998) 387.
[26] M.M. Günter, T. Ressler, R.E. Jentoft, B. Bems, J. Catal. 203 (2001) 133.